

Is the ‘Azores Hotspot’ a Wetspot? Insights from the Geochemistry of Fluid and Melt Inclusions in Olivine of Pico Basalts

**NICOLE MÉTRICH^{1*}, VITTORIO ZANON², LAURA CRÉON^{1,3},
ANTHONY HILDENBRAND^{3,4}, MANUEL MOREIRA¹ AND
FERNANDO ORNELAS MARQUES⁵**

¹INSTITUT DE PHYSIQUE DU GLOBE, SORBONNE PARIS-CITÉ, UNIVERSITÉ PARIS DIDEROT, UMR-CNRS 7154, PARIS, FRANCE

²CENTRO DE VULCANOLOGIA E AVALIAÇÃO DE RISCOS GEOLÓGICOS, UNIVERSIDADE DOS AÇORES, PONTA DELGADA, PORTUGAL

³UNIV PARIS-SUD, LABORATOIRE IDES, UMR8148, ORSAY, F-91405, FRANCE

⁴CNRS, ORSAY, F-91405, FRANCE

⁵UNIVERSIDADE DE LISBOA, LISBOA, PORTUGAL

RECEIVED JULY 12, 2013; ACCEPTED NOVEMBER 4, 2013

The concept of an ‘Azores mantle plume’ has been widely debated, and the existence of an Azores hotspot questioned. In an effort to shed new light on this controversy, we present He isotope and major, trace and volatile element compositions for basaltic scoriae from five monogenetic cones emplaced along the fissure zone of Pico Island, the youngest island of the Azores archipelago. The bulk scoriae and lavas are moderately alkaline basalts, and their He isotope ratios, determined on olivine crystals, vary between 10.2 and 11.1 ± 0.1 R_a. In contrast, melt inclusions hosted in olivine (Fo_{76–83.5}) span a large range of compositions (K₂O = 0.7–1.7 wt %; Ce = 32–65 ppm; Nb = 21–94 ppm), which extends the compositional field of lavas erupted along the Pico fissure zone. This chemical evolution is predominantly controlled by polybaric fractional crystallization. Most melt inclusions share similar enrichments in large ion lithophile and light rare earth elements, and trace element ratios (La/Sm, La/Yb, Sr/Nd, Ta/Th, Zr/Y) with their bulk-rocks. Only a few of them differ in their lower contents of incompatible elements and La/Sm, Li/Ta and Na/K ratios, a feature that is ascribed to distinct conditions of melting. As a whole, the melt inclusions preserve high and variable volatile contents, and contain up to 1.8–2.0 wt % of H₂O and 0.4 wt % of CO₂. The total fluid pressures, retrieved from the dissolved CO₂ and H₂O concentrations, and the P_{CO2} from fluid

inclusions, indicate magma ponding and crystallization at the crust–mantle boundary (ca. 18 km deep). The H₂O/Cl and H₂O/Ce ratios in the inferred parental undegassed basalts of the Pico fissure zone average 0.036 ± 0.006 and 259 ± 21, respectively. The latter value is significantly higher than that reported for typical mid-ocean ridge basalts from the southern Mid-Atlantic Ridge, but is similar to published ratios for submarine undegassed basalts from the Azores platform. Combining the calculated compositions of Pico primary magmas formed by low degrees of melting with recent geophysical data for the Azores, we propose a model for Azores magma generation involving the decompression melting of a water-enriched mantle domain (H₂O = 630–570 ppm) with an estimated temperature excess of ≤120°C with respect to the Mid-Atlantic Ridge.

KEY WORDS: Azores; Pico basalts; melt inclusions; trace and volatile elements; helium isotopes; decompression melting

INTRODUCTION

The Azores oceanic intra-plate archipelago is the emerged part of the Azores Platform, a region of elevated

*Corresponding author. Present address: Institut de Physique du Globe de Paris, Géologie des Systèmes Volcaniques, 1, rue Jussieu, 75238 Paris cedex 05, France. E-mail: metrich@ipgp.fr

topography transected by the Mid-Atlantic Ridge (MAR) axis and bounded to the north by the slow-spreading Terceira Rift and to the south by the Azores–Gibraltar Fracture Zone. At the junction between three major lithospheric plates—the North American, African and Eurasian plates—the Azores islands are thus located in a complex tectonic setting characterized by anomalously thick crust (≥ 8 km; Luis *et al.*, 1998; Gente *et al.*, 2003; Dias *et al.*, 2007; Georgen & Sankar, 2010; Silveira *et al.*, 2010) and the presence of ‘V-shaped’ ridges along the adjacent MAR (e.g. Vogt, 1979; Cannat *et al.*, 1999; Escartín *et al.*, 2001).

The Azores have long been considered as a typical example of hotspot–ridge interaction (e.g. Schilling, 1975; White & Schilling, 1978; Cannat *et al.*, 1999; Dixon *et al.*, 2002; Moreira & Allègre, 2002), with variable He isotopic ratios bracketing the mid-ocean ridge basalt (MORB) values of $8 \pm 1 R_a$ (e.g. Moreira *et al.*, 1999; Madureira *et al.*, 2005; Jean-Baptiste *et al.*, 2009). The Azorean basalts show an increasing enrichment in incompatible elements and radiogenic Sr–Nd–Pb signatures with increasing distance from the MAR (e.g. Turner *et al.*, 1997; Moreira *et al.*, 1999; Bourdon *et al.*, 2005; Beier *et al.*, 2008, 2010). It has also been proposed that Azores-type mantle melts could have interacted with depleted MORB-source mantle along the MAR, at very low extents of melting (Gale *et al.*, 2011). The mantle geochemical heterogeneity beneath the Azores archipelago has been widely discussed, mainly focusing on São Miguel, the easternmost island in the Terceira Rift, and associated with the recycling of underplated basalts into the oceanic mantle (e.g. Beier *et al.*, 2007; Elliott *et al.*, 2007; Moreira *et al.*, 2012).

The enrichment in volatiles, specifically water, of Azores magmas was first recognized by Schilling *et al.* (1980) in submarine basalts of the platform, which have high H₂O/Ce ratios relative to typical MORB (Michael, 1995). The water anomaly of the Azorean mantle domain was associated with recycling of old oceanic crust (Dixon *et al.*, 2002). The addition of H₂O to the mantle, together with a small temperature anomaly, are the key parameters to induce polybaric hydrous melting and fractionation that led Bonatti (1990) and Asimow *et al.* (2004) to question the concept of an Azores hotspot and the associated thermal anomaly. Alternative models propose the mantle partial melting beneath the Azores to be caused by the stretching of the lithosphere along transtensive fault systems and differential stresses generated by the segmentation of the MAR (e.g. Luis *et al.*, 1994; Marques *et al.*, 2013).

Retrieving the initial volatile content of the Azores primary magmas and the mantle melting temperature is thus of prime importance, but is often hampered by the absence of true primary melts because of olivine and pyroxene crystallization at high pressure (e.g. Genske *et al.*, 2012; Zanon *et al.*, 2013). Moreover, the volatile dataset

available from the literature is mainly based on MAR basalts emplaced on the sea floor. Here, we focus on the explosive products from monogenetic cones and subaerial lava flows emplaced along the Pico eastern fissure system and, more specifically, on melt inclusions hosted in olivine representative of the early stages of magma crystallization. We provide new He isotope data, which, together with bulk-rock trace element compositions, demonstrate that our sample set is representative of the magmas emplaced along the Pico fissure zone. This study raises the question of the significance of helium isotope ratios higher than those of MORB, but significantly lower than typical values from hotspots. We combine data from melt and CO₂-rich fluid inclusions with bulk-rock geochemistry to estimate the *P*–*T* conditions of magma ponding and evolution. Our results indicate direct transfer of magma batches from the mantle–crust transition or deeper, the presence of a water-rich mantle, and also variable conditions of mantle partial melting.

GEOLOGICAL SETTING AND SAMPLE DESCRIPTION

Pico, located at 38.2–38.4°N, is one of the nine volcanic islands of the Azores archipelago (36.8–39.9°N). Together with the nearby island of Faial it forms a ~160 km long volcanic ridge oriented WNW–ESE (Fig. 1), which lies on *ca.* 10 Myr old oceanic lithosphere (e.g. Luis *et al.*, 1994; Cannat *et al.*, 1999). Pico island, the youngest of the archipelago, consists of basalts (França *et al.*, 2006) and the oldest subaerial lava flows are younger than 200 ka (A. Hildenbrand, unpublished data). It is formed by three main volcanic systems: the Topo–Lajes complex, where the oldest age was found; the Pico Ridge complex (Planalto da Achada Fissure Zone), which is subaerial for *ca.* 30 km and extends underwater for *ca.* 100 km (Stretch *et al.*, 2006), and where the eruptive activity continued until AD 1562; and the Pico stratovolcano, which peaks at 2350 m and last erupted in AD 1720.

Here we focus on five monogenetic cones (Sc11A–E), which were sampled during a field mission in 2012, and were built along the Pico axial fissure system (Fig. 1) on top of young lava flows dissected by an active slump on its southeastern flank (Hildenbrand *et al.*, 2012a). One of them (Sc11C) is located close to the slump headwall. These cones have not yet been dated, but their very well-preserved morphology suggests that they were generated no more than a few thousand years ago. Excess in ²²⁶Ra measured in two basalts from the Pico fissure system (Prytulak & Elliott, 2009) provides indirect evidence for their relative young age (<8000 years). The fresh scoriae, which were specifically collected to obtain the most rapidly quenched samples for melt inclusion study, come from unwelded, poorly stratified vesicular lapilli and scoria

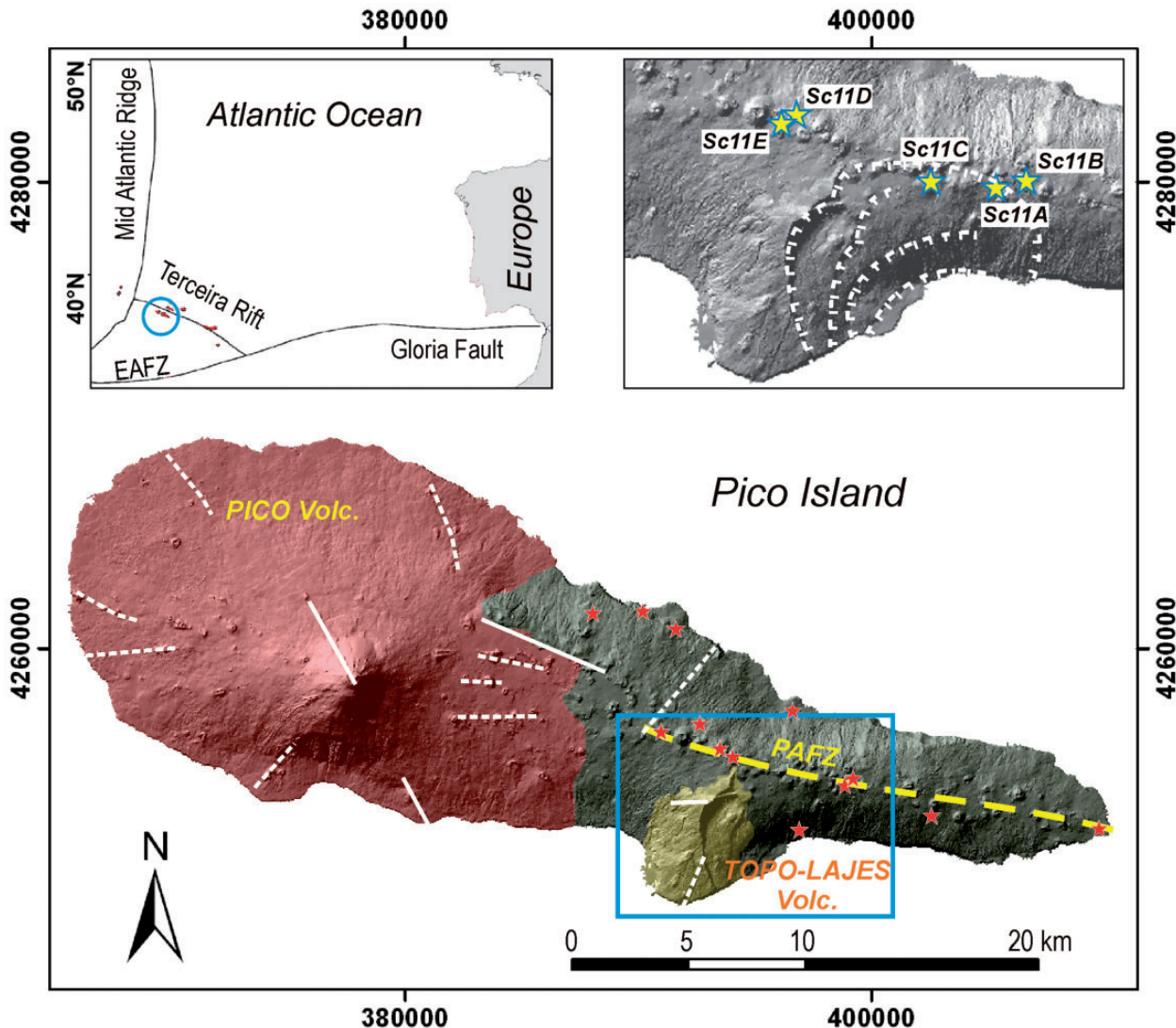


Fig. 1. Digital elevation model of the island of Pico showing the main morphological features, tectonic discontinuities (white lines) and the fissure zone system of Planalto da Achada (PAFZ), simplified from Madeira & Brum da Silveira (2003). The shaded areas correspond to the three volcanic complexes. Stars indicate the locations of the lava samples analyzed in this study. The left-hand inset shows the location of the Azores archipelago and the main geostructural lineaments. EAFZ, East Azores Fracture Zone. The right-hand inset represents the studied area, with scarp faults and active slumps reproduced from Hildenbrand *et al.* (2012a). Stars mark the location of monogenetic cones sampled for He isotope measurements in olivine crystals and geochemical analysis of melt inclusions and bulk-rocks.

beds, emplaced during Strombolian activity. The deposit grain size varies from 2–3 cm in the largest clasts to millimeters in the smallest. Their mineral assemblage comprises olivine, plagioclase and clinopyroxene. We specifically studied euhedral olivine crystals, hand-picked from both 0.5–1.0 and 1.0–2.0 mm grain-size fractions to retrieve as much information as possible on the earliest stage of magma history. Olivine commonly contains isolated, rounded melt or glass inclusions up to 300–400 µm in size, with a single or several shrinkage bubble(s) and occasionally sulfide globules. Melt inclusions are generally preserved as yellowish glass; in some cases their dark

brown color is related to the presence of numerous sub-micrometer-sized nuclei, which appeared upon cooling and disappeared during heating at 1 atm. However, we stress that measurements were made on naturally quenched, unheated melt inclusions. Trails of pseudo-secondary CO₂-rich fluid inclusions, aligned along healed fractures, are ubiquitous in the three mineral phases, but were measured in olivine crystals only.

To complement the geochemical study, 13 new basaltic lava samples were also collected along the subaerial fissure zone (Fig. 1). They typically display a low amount of phenocrysts (<18%) of olivine, plagioclase and

clinopyroxene in order of decreasing abundance, and only very rare megacrysts (≥ 5 mm; most probably antecrysts; Zanon & Frezzotti, 2013). Microtextures range from intergranular to seriate, and the groundmass is typically microcrystalline.

ANALYTICAL PROCEDURES

Major and trace elements in bulk-rocks

Major and trace element analyses of the scoria samples (Sc1A–E) were carried out at the Centre de Recherches Pétrographiques et Géochimiques (SARM) in Nancy (France), using inductively coupled plasma optical emission spectroscopy (ICP-OES) and inductively coupled plasma mass spectrometry (ICP-MS), respectively (Carignan *et al.*, 2001). The major and trace element compositions of the lavas were measured at the Activation Laboratories (Ancaster, Ontario, Canada) as described by Zanon *et al.* (2013). Major and trace element data for bulk-rocks from the Pico fissure zone are reported in Supplementary Data Electronic Appendix 1 (supplementary data are available for downloading at <http://www.petology.oxfordjournals.org>).

Melt inclusions, CO₂-rich fluid inclusions and their host olivine crystals

Transmission infrared spectroscopy measurements of CO₂ and H₂O

Carbon and water were analyzed first in double face polished melt/glass inclusions by Fourier transform infrared spectroscopy. We used a Nicolet Magna-IR 550 spectrometer, equipped with a Globar source, an MCT/A detector cooled with N₂, and a X-KBr beam splitter, which is coupled with a Spectra-Tech microscope (IPGP). Concentrations were calculated according to Beer–Lambert's law: C (wt %) = $[(100AM)/(\varepsilon pe)]$, where A is the absorbance, M the molar mass (g mol⁻¹), ε the molar absorptivity (l mol⁻¹ cm⁻¹), e the thickness (cm), and ρ the glass density. The doubly polished wafer thickness, which typically varied between 35 and 100 µm, was measured with an error of ± 2 –3 µm using a Mitutoyo digital comparator and optical microscope. The glass density was calculated following Lange & Carmichael (1990) with a H₂O molar volume of 12 l mol⁻¹ (Richet *et al.*, 2000). The total amount of dissolved water (H₂O_{mol}+OH⁻) was derived from the broad band at 3535 cm⁻¹, using an absorption coefficient of 62·81 mol⁻¹ cm⁻¹ (Mercier *et al.*, 2010). Carbon concentration was determined by measuring the peak height at 1520 cm⁻¹ on the background-subtracted spectra, and after deconvolution taking into account the contribution of the molecular H₂O peak at 1630 cm⁻¹. The absorption coefficient was calculated using the equation $\varepsilon^{1520} = 451 - 342[\text{Na}/(\text{Ca} + \text{Na})]$, according to Dixon

& Pan (1995). The relative errors are estimated to be better than 10% for H₂O and 15% for CO₂.

Major and volatile element analyses

Major elements in glasses and minerals were analyzed in three scoria samples (Sc1 C, D and E) using a Cameca SXFive electron probe (Camparis, Paris, France). In melt inclusions they were measured with a 10 nA defocused beam and a counting time varying from 10 to 20 s. The concentrations of S, Cl and P were determined with a 30 nA defocused beam and a counting time of 120 s on peak. Fluorine was analyzed by coupling LTAP and TAP crystals, with 50 nA beam current, 15 µm beam size, and 100 s counting time. The analysis accuracy was checked against the international standard Vg2, and internal reference natural obsidians (Electronic Appendix 2a). The relative errors are <5% for S and F and <8% for Cl. The detection limits are 50 ppm for S and Cl, and <100 ppm for F. Minerals were analyzed with a focused beam, a beam current of 10–40 nA and a counting time varying from 10 to 20 s.

Trace element analyses

Melt inclusions were analyzed for trace elements by laser ablation (LA)-ICP-MS, using a 193 nm ArF excimer laser ablation system (Resonetics M50) coupled to a 7500cs Agilent ICP-MS system at the Laboratoire Magmas et Volcans (Clermont-Ferrand, France), with helium as the ablation gas. Samples were analyzed using a laser repetition rate of 2–3 Hz, 44 µm laser spot diameter and pulse energy of 6 mJ (14 J cm⁻²). The background was measured for 30 s before ablation, and each analysis lasted \sim 80 s. Measurements were calibrated against NIST 612 glass standard (Gagnon *et al.*, 2008), using CaO as the internal element reference. Reproducibility and accuracy of the analyses were checked against the BCR2-G glass international standard (Electronic Appendix 2b), which was recurrently analyzed during every analytical session, and are better than 10%. Data reduction was performed using the Glitter software (Van Achterbergh *et al.*, 2001).

Fluid inclusion microthermometry

A Linkam THMS600 heating–freezing stage was used to measure the phase transitions in CO₂-rich fluid inclusions, which homogenized in the liquid phase in our samples. After freezing the fluid at $< -75^\circ\text{C}$, the inclusions were slowly heated to the triple point temperature check (-56.6°C for pure CO₂) with a heating rate of 0.5–2 °C min⁻¹. Final homogenization occurred to the liquid phase (T_{hL}). The CO₂ density and P_{CO_2} were calculated following Span & Wagner (1996) and Stern & Pitzer (1994), respectively, for a magma temperature of $1155 \pm 15^\circ\text{C}$ as assessed for Pico basalts (Zanon & Frezzotti, 2013). We verified this latter estimate by modeling the basalt

crystallization path at 500 MPa, under the quartz–fayalite–magnetite (QFM) buffer, using MELTS (Ghiorso & Sack, 1995), starting from the basalt liquidus temperature down to the crystallization of the olivine Fo_{80-82} . A difference of 10–15°C will shift the pressure values of $\pm 3-5$ MPa in the domain of interest.

Helium measurements

Helium concentrations and isotope ratios were measured at IPGP, on olivine crystals that were hand-picked from the five scoria samples (Sc11A–E), in the 1–2 mm size fraction, after removal of the external glass with dilute HF and cleaning with distilled water and alcohol. In olivine crystals in samples Sc11C and D data were also acquired for smaller crystals (0.5–1 mm). The gas was extracted by crushing under vacuum, purified using one Ti getter at a temperature of 800°C and one SAES getter at room temperature. After purification, the noble gases were trapped on activated charcoal at 10 K. Helium and neon were introduced successively and analyzed for their isotopic composition using a Noblesse mass spectrometer (Nu Instruments). We report He data only; the isotopic data for Ne will be presented elsewhere. The measurements were calibrated against an internal reference gas with a

${}^4\text{He}/{}^3\text{He}$ ratio of 95210 ± 440 [$R/R_a = ({}^3\text{He}/{}^4\text{He})_{\text{sample}} / ({}^3\text{He}/{}^4\text{He})_{\text{atmosphere}} = 7.59 \pm 0.04$; $R_a = 1.384 \times 10^{-6}$] (Madureira *et al.*, 2005).

RESULTS

Bulk-rock chemistry and olivine He data: a relative homogeneity

Bulk scoria samples (Sc11A–E) have similar alkali basaltic compositions, with average values of 46.6 wt %, 1.2 wt % and 7 wt % for SiO_2 , K_2O and MgO , respectively (Electronic Appendix 1). Hence, these basalts are not primary mantle-derived magmas and have experienced variable degrees of fractional crystallization. Their trace element patterns are typical of basalts erupted along the Pico fissure zone system (Fig. 2a). They are relatively enriched with respect to both normal and enriched MORB, and display heavy rare earth element (HREE) fractionation.

The ${}^4\text{He}$ concentrations measured in olivine crystals from the same scoria samples vary significantly from 3.4 to $9.8 \times 10^{-8} \text{ cm}^3 \text{ STP g}^{-1}$, without systematic difference between the olivine grain-size fractions (Table 1). These

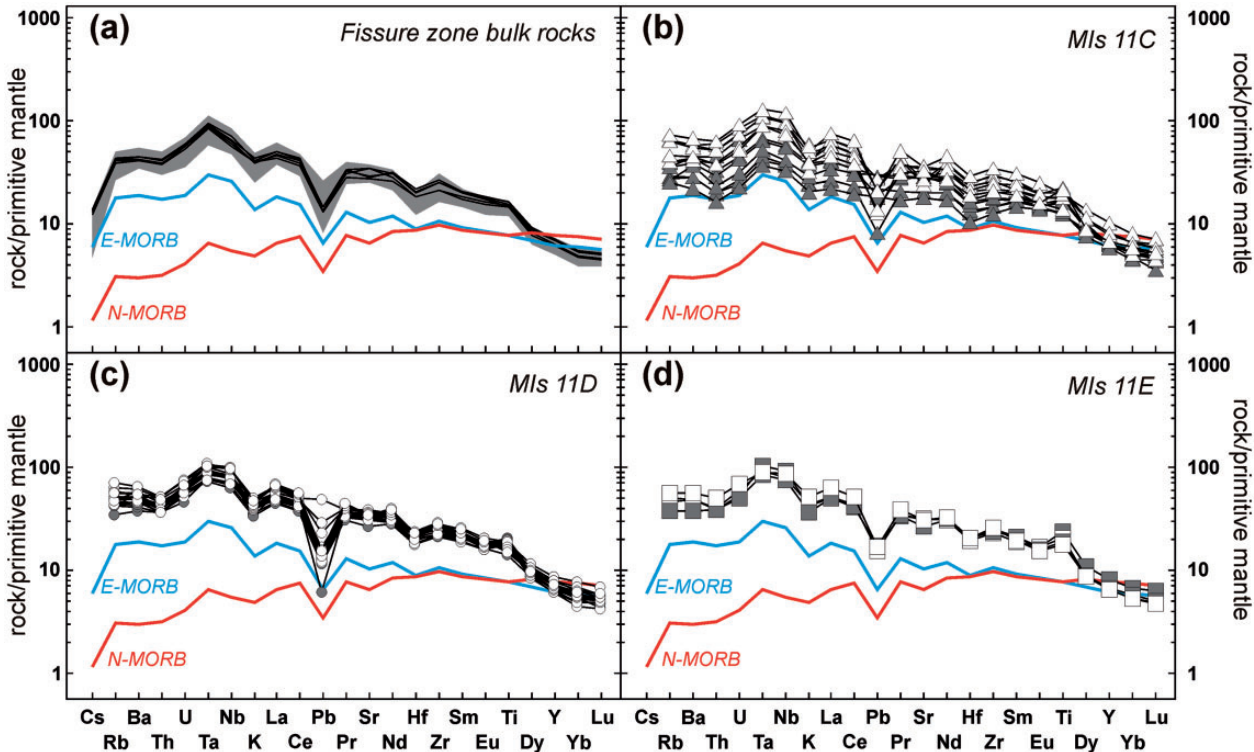


Fig. 2. Trace element patterns normalized to primitive mantle (McDonough & Sun, 1995), for bulk-rocks (a) and melt inclusions (b–d). In (a), the thick black lines refer to the bulk scoria (Sc11A–E) from the five monogenetic cones. The grey area delineates the range of basaltic lavas emplaced along Pico fissure zone. (b)–(d) illustrate the melt inclusion patterns of samples Sc11C, Sc11D and Sc11E; filled and open symbols refer to melt inclusions in olivine $\text{Fo}_{\geq 80}$ and $\text{Fo}_{<80}$, respectively. Data for enriched MORB (E-MORB) and normal MORB (N-MORB) are from Gale *et al.* (2013).

Table 1: Helium concentrations [$\text{in } 10^{-8} \text{ cm}^3 (\text{STP}) \text{ g}^{-1}$] and isotopic compositions of olivine crystals from Pico monogenetic cones

Sample	Grain size (mm)	${}^4\text{He} \times 10^{-8}$	R/R_a	\pm
Sc11-A	1-2	3.93	10.55	0.09
Sc11-B	1-2	3.43	10.18	0.09
Sc11-C	1-2	9.44	10.18	0.08
Sc11-C	0.5-1	4.98	10.30	0.13
Sc11-D	1-2	9.75	11.09	0.09
Sc11-D	0.5-1	9.76	10.62	0.11
Sc11-E	1-2	3.56	10.89	0.10

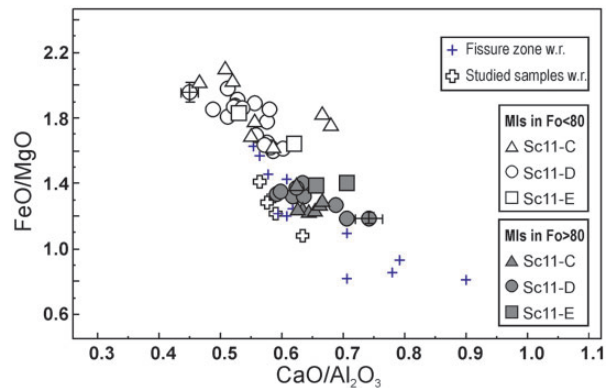


Fig. 3. Variation of $\text{CaO}/\text{Al}_2\text{O}_3$ vs FeO/MgO in bulk-rocks and olivine-hosted melt inclusions from the Pico fissure zone. The melt inclusions hosted in olivine $\text{Fo}_{\geq 80}$ plot in the lava domain whereas those in olivine $\text{Fo}_{<80}$ are clearly more evolved than the bulk-rocks. The lavas significantly enriched in MgO (lowest FeO/MgO ratios) are olivine cumulative. (See text for further details.)

values are significantly higher than those reported for olivine crystals in extensively degassed lava samples, which have concentrations predominantly between ≤ 1.0 and $4.0 \times 10^{-8} \text{ cm}^3 \text{ STP g}^{-1}$ (Moreira & Allègre, 2002). Rapid cooling of the scoria could have prevented extensive He diffusion within the olivine upon eruption without isotopic fractionation. The helium isotopic ratios of the scoria samples fall in a narrow range of values from 10.2 to $11.1 \pm 0.1 R_a$, typical of Pico Island (on average $11.5 R_a$; Moreira *et al.*, 2002), but differ from MORB values (${}^4\text{He}/{}^3\text{He} \sim 90\,000 \pm 10\,000$ or $\sim 8 \pm 1 R_a$; e.g. Parman, 2007). The scoria samples studied in detail here for melt and fluid inclusions are thus representative of the recent magmatism of the Pico fissure system.

Mineral and melt inclusion chemistry: a wide compositional spectrum

The basaltic scoria contain olivine ($\text{Fo}_{73.7-83.5}$), clinopyroxene (Mg number varying from 0.86–0.78 in the core to 0.81–0.77 in the rim) and plagioclase ($\text{An}_{82.3-70.3}$ in the core to $\text{An}_{65.7-66.5}$ in the rim) phenocrysts. We observed rare plagioclase megacrysts ($\text{An}_{57.6-61.6}$). Systematic analysis of olivine shows a similar compositional range in the three samples Sc11D, E and C. Typically, olivine $\text{Fo}_{\geq 80}$ is normally zoned, with the rim composition recording late-stage equilibration. In sample Sc11C, olivine crystals Fo_{74-77} are reversely zoned up to Fo_{82} , indicative of mixing between magma batches with distinct compositions and/or temperatures. Olivine $\text{Fo}_{77-74.7}$ enclosed in clinopyroxene (Mg number 0.81–0.79), testifies to the last stage of crystallization.

Melt inclusions were specifically analyzed in olivine and their compositions were corrected for post-entrapment crystallization (PEC). There is little constraint on the redox conditions of the Pico basalts and we thus used a

range of f_{O_2} and Fe^{3+} proportions. For QFM buffer conditions, a temperature of 1155°C , and a K_D value of 0.30 (Toplis, 2005), the extent of PEC is calculated to be below 4% (Electronic Appendix 3). The results are comparable for a K_D value of 0.32 under slightly more oxidizing conditions (Ni–NiO).

Melt inclusions hosted in olivine $\text{Fo}_{\geq 80}$ plot in the domain of Pico bulk samples, with comparable $\text{CaO}/\text{Al}_2\text{O}_3 (>0.6)$ and $\text{FeO}/\text{MgO} (<1.4)$ ratios (Fig. 3). There is no significant difference between the three studied samples (Sc11D, E, C). They share similar trace element patterns with the Pico lavas, whereas melt inclusions in $\text{Fo}_{<80}$ olivine are enriched in trace elements (Fig. 2b–d), a feature consistent with their more evolved nature.

Trace elements allow us to discriminate the processes that control the magma and bulk sample chemistry. Pico melt inclusions and bulk lavas belong to the same series of evolution, as deduced from positive correlations between Rb, Th and Ta going through zero (Fig. 4a and b), and the constant ratios between incompatible elements such as Rb/Ta, Th/Ta and Ce/K₂O (Table 2). Strontium correlates with Ta, except in the most evolved compositions (Ta >3.5 ppm; Fig. 4c). Crystal fractionation is demonstrated in the plots of Li and Sc vs Ta (Fig. 4d and e), showing the effective role of clinopyroxene fractionation in the Sc decrease. However, crystal fractionation during magma evolution cannot account for the variation of the incompatible elements (i.e. $1.4 < \text{Ta} < 3.3$ ppm) for a very limited range of Li, Sc and Ni contents (Fig. 4d–f), and thus for magmas at the same stage of evolution. From the most primitive basaltic inclusions (in olivine $\text{Fo}_{80-83.5}$), it emerges that (1) Pico magmas display a significant range in Th, Ta, Nb, Ce and K₂O concentrations, (2) they are enriched with respect to both normal- and enriched-MORB, and (3) their La/Sm ratio averages at 4.0 ± 0.3 , which is

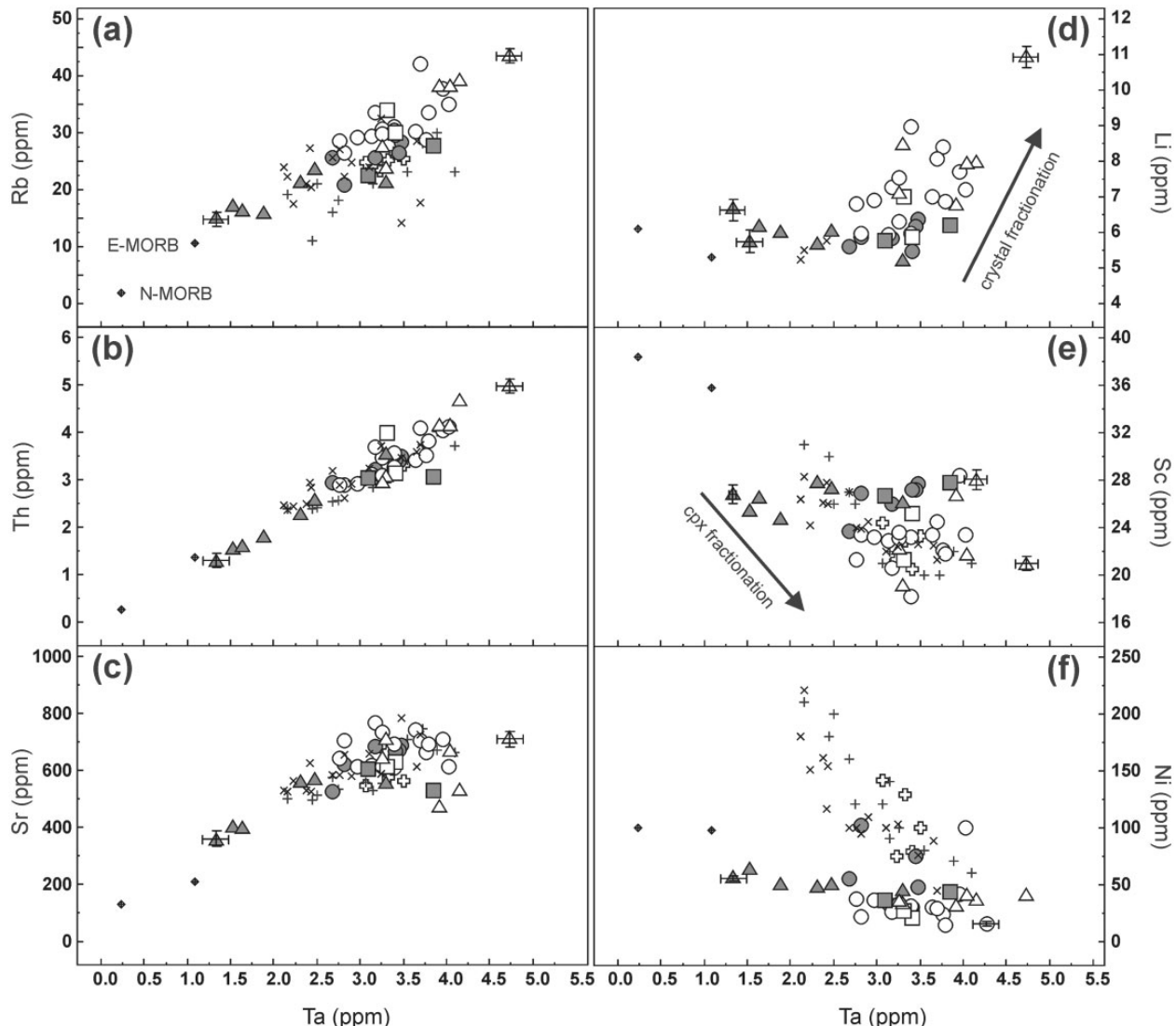


Fig. 4. Trace element variations in olivine-hosted melt inclusions and bulk-rocks from the Pico fissure zone. The data for subaerial lavas (crosses) are from Beier *et al.* (2012) and those for enriched MORB (E-MORB) and normal MORB (N-MORB) from Gale *et al.* (2013). Symbols as in Fig. 3.

the typical value of basalts emplaced along the Pico fissure zone system, with exception of the Sc11C sample. In the latter, melt inclusions in equilibrium with olivine (Fo_{82-83}) show a wide chemical range. They extend the domain of Pico magmas towards relatively low incompatible element contents (Fig. 5a and b), and low La/Sm , La/Yb , $\text{K}_2\text{O}/\text{Na}_2\text{O}$ and Zr/Y ratios (Table 2). An average La/Sm ratio of 2.5 ± 0.1 is comparable with those reported for MAR basalts dredged between 35 and 45°N ($1 < \text{La}/\text{Sm} < 3$; Schilling, 1975; Michael, 1995). Hence, Pico melt inclusions preserve the initial chemical heterogeneity of the magma batches, with possible mixing between batches generated by fractional melting in the same mantle volume, or reflecting distinct extents of partial mantle melting.

Some lavas are significantly enriched in compatible elements such as Ni (Fig. 4f), which confirms their cumulative nature (olivine \pm clinopyroxene) in agreement with their low FeO/MgO ratio (<1 ; Fig. 3). The positive correlation between Ni and MgO (not shown) demonstrates that high-Ni lava samples are not representative of true primary magmas, which are never (or very rarely) erupted. This is an important feature for mantle melting temperature calculations, as discussed further below.

Dissolved volatiles and melt saturation pressures

The analyzed melt inclusions from Pico have variable total volatile contents from ~ 2.5 to <1 wt %, with H_2O being the dominant species (Electronic Appendix 3). Sulfur

Table 2: Mean ratio values of melt inclusions and bulk-rocks

	Ta/ Th	Rb/ Ta	Ce/ K ₂ O*	K ₂ O/ Na ₂ O	La/ Sm	La/ Yb	Sr/ Nd	Zr/Y
<i>Melt inclusions—dominant population</i>								
Mean (22)†	1.00	8.8	6.2	0.33	4.1	13.9	16.1	8.6
SE‡	0.03	0.5	0.3	0.03	0.1	0.8	0.6	0.4
<i>Melt inclusions§</i>								
Mean (4)	1.02	10.2	5.7	0.17	2.5	7.8	16.4	6.0
SE	0.03	1.3	0.3	0.03	0.1	1.1	0.8	1.0
<i>Bulk scoriae</i>								
Mean (5)	0.95	7.5	5.8	0.33	3.9	13.4	16.7	8.7
SE	0.02	0.3	0.3	0.01	0.1	0.3	1.9	0.3
<i>Bulk lavas</i>								
Mean (19)	1.02	7.0	6.0	0.33	4.2	14.9	17.5	9.5
SE	0.03	0.5	0.5	0.02	0.1	0.4	0.7	0.3

*Ratio $\times 10^3$.

†Mean ratio. The number of analyses (*n*) is given in parenthesis.

‡Standard error (SE = $2\sigma/\sqrt{n}$).

§Melt inclusions departing from the general trend of Pico basalt evolution.

varies little during magma evolution at sulfide saturation, except in open embayments ($S < 500$ ppm) in contact with the surrounding magma (Fig. 6a). Sulfur contents range from 1390 to 1710 ppm (1517 ± 130 ppm on average) in samples Sc11D and E, and from 1195 to 1954 ppm (1488 ± 205 ppm on average) in Sc11C scoriae. Chlorine co-varies with K₂O ($Cl/K_2O = 0.05$) and its concentration ranges from 326 to 853 ppm. The widest variation is observed in sample Sc11C (Fig. 6b).

Melt inclusions also record variable contents of H₂O (from <0.8 to 2.0 wt %) and CO₂ (from 662 to 4039 ppm). The largest ranges of concentrations were recorded in sample Sc11C, whereas one embayment (Sc11D-6b) has the lowest H₂O concentration (~ 0.4 wt %). There is no clear relationship between inclusion size and H₂O content for an average diameter larger than 80–100 µm (Electronic Appendix 3). Figure 7 demonstrates that most inclusions have lost more than 30% of their initial water content, possibly related to several different processes as briefly discussed below. However, the overall dataset allows us to define an H₂O content upper envelope (or limit) that delineates a positive correlation between H₂O and Ce in melt inclusions differing in their H₂O concentrations (Fig. 7a). The corresponding H₂O/Ce ratios range from 226 to 309 (Fig. 7b) and average at 259 ± 21 ($2\sigma/\sqrt{n}; n=10$), which confirms the closely similar behaviour of H₂O and Ce during mantle partial melting and subsequent melt evolution. A similar conclusion can be

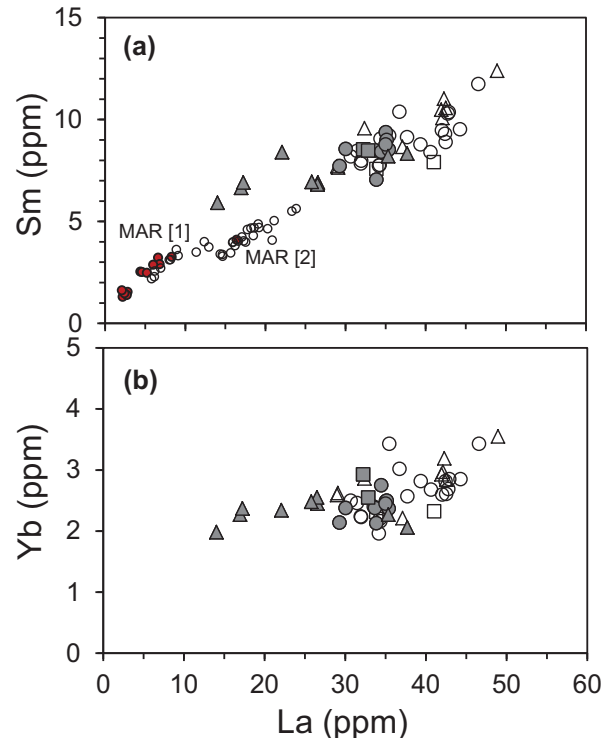


Fig. 5. Variation of Sm (a) and Yb (b) vs La in Pico bulk-rocks (lavas and scoria) and olivine-hosted melt inclusions from the monogenetic cones Sc11D, E, C, [1], MAR submarine basalts dredged between 35 and 45°N ($1 < La/Sm < 3$; Schilling, 1975; Michael, 1995); [2], MAR basalts between 37° and 39°N (Gale *et al.*, 2011). Symbols as in Fig. 3.

drawn for H₂O and La, as Ce and La are very well correlated ($Ce/La = 2.18 \pm 0.02$; $R^2 = 0.987$). The H₂O/Cl and H₂O/K₂O ratios average at 0.036 ± 0.06 and 1.6 ± 0.1 , respectively.

For every melt inclusion we calculated the saturation fluid pressure ($P_{CO_2} + P_{H_2O}$) from its dissolved CO₂ and H₂O content using the method of Papale *et al.* (2006), for QFM redox conditions and 1155°C. The highest pressure and the largest range of values (from 468 down to 87 MPa) were found in sample Sc11C, whereas most fluid pressures cluster between 350 and 200 MPa in samples Sc11D and Sc11E (Electronic Appendix 3). However, the thermodynamic model developed by Papale *et al.* (2006) has a tendency to overestimate CO₂ solubility and thus to underestimate the saturation pressure of CO₂-rich melts with low to moderate H₂O contents (Shishkina *et al.*, 2010). Taking the possible diffusive loss of CO₂ in the shrinkage bubble into account, the fluid pressures derived from the dissolved volatile concentrations are underestimated.

CO₂-rich fluid inclusions and related pressures

CO₂-rich fluid inclusions are present in each mineral phase, but olivine potentially offers the best chance to

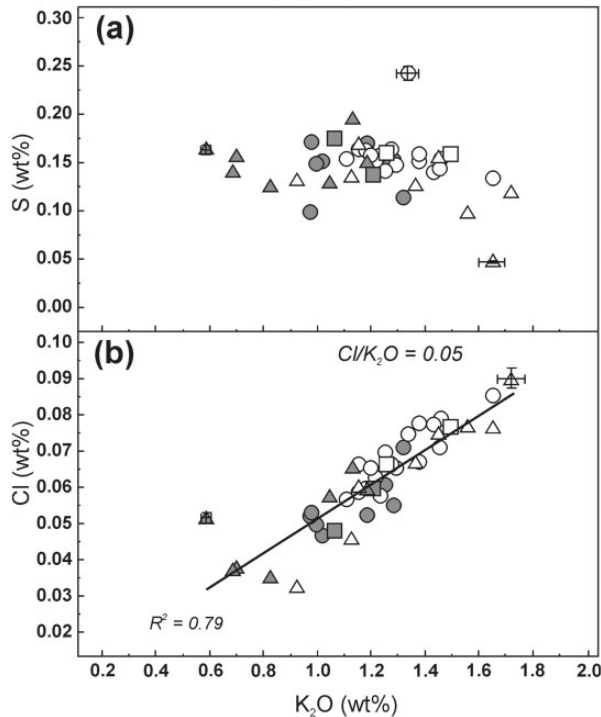


Fig. 6. Variation of sulfur (a) and chlorine (b) vs K_2O in olivine-hosted melt inclusions in scoria from the Pico monogenetic cones. Symbols as in Fig. 3.

constrain the highest pressures and to compare the P_{CO_2} values to the total fluid pressures deduced from the amount of CO_2 and H_2O dissolved in the melt inclusions. About 240 measurements were performed on pseudo-secondary fluid inclusions disposed along healed fractures within olivine (Fig. 8a), covering almost the whole range of compositions from Fo_{82} to Fo_{75} (Electronic Appendix 4a). These inclusions are perfectly rounded, with a diameter $\leq 25\ \mu m$. Frozen inclusions melted instantaneously between -56.8 and $-56.6^\circ C$ (± 0.1) that is, within the error limits, the temperature of the CO_2 triple point ($-56.6^\circ C$). The CO_2 melting temperature was verified only in the largest inclusions, as light reflection in the smallest ones hampered any measurements. At room temperature one (L) or two (L + V) phases are present and inclusions homogenized into a liquid phase between 23.1 and $30.6^\circ C$ in the Sc1ID sample, between 17.1 and $30.4^\circ C$ in Sc1IE, and between 15.4 and $22.3^\circ C$ in Sc1IC (Fig. 8b). Inclusions along the same trail homogenized at the same temperature. The corresponding P_{CO_2} values range from 259 to 526 MPa (Fig. 8c), as reported for other basaltic lavas from the Pico fissure zone (Zanon & Frezzotti, 2013). The highest pressures were recorded in sample Sc1IC, with values that average at $470 \pm 32\text{ MPa}$ compared with 353 ± 34 and $369 \pm 69\text{ MPa}$ in samples Sc1ID and E, respectively. Water may have been lost at an early stage, but the H_2O content of the fluid phase in equilibrium with the silicate portion

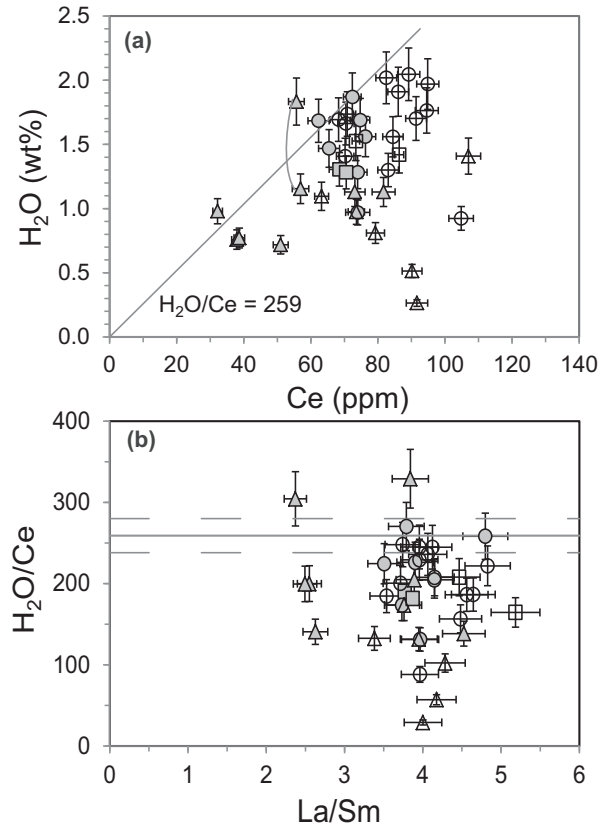


Fig. 7. (a) Variation of H_2O vs Ce in olivine-hosted melt inclusions in scoria from the Pico monogenetic cones. The two data points connected by a thin line correspond to melt inclusions within the same crystal. (b) Variation of H_2O/Ce vs La/Sm . Symbols as in Fig. 3.

of the melt inclusion at magmatic temperature is calculated to be $\leq 0.15\text{ mol }%$. This fraction of H_2O has a minimal influence on our fluid pressure estimates. We stress that P_{CO_2} derived from secondary fluid inclusions indicates the last event of pressure re-equilibration. A high-density frequency maximum is identified in sample Sc1IC, which most probably reveals a long period of magma ponding at high pressure, as proposed for La Palma peridotite xenoliths by Hansteen & Klügel (2008). Following those researchers, the wide distribution of Sc1IE data and, to a limited extent, data for Sc1ID demonstrates re-equilibration during magma ascent without a further long period of magma ponding.

DISCUSSION

High-pressure magma ponding

Figure 9 illustrates the behavior of H_2O and CO_2 , which deviates from the theoretical equilibrium degassing trend, calculated under closed-system conditions (CSD^b) with 1 wt % of free gas phase. As often observed in basaltic

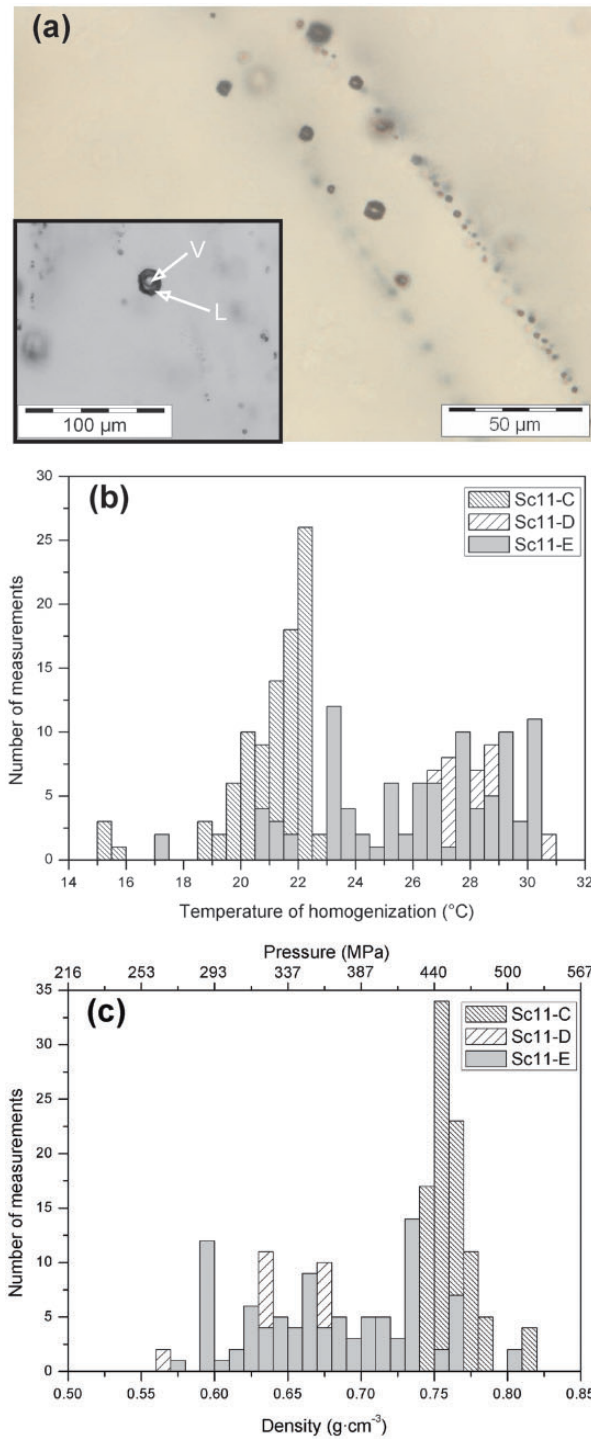


Fig. 8. (a) Photomicrograph showing CO₂-rich fluid inclusions aligned along a healed fracture in olivine from a monogenetic scoria cone of the Pico fissure zone. (b) Distribution of the homogenization temperature in the liquid phase for samples Sc11C, D and E. (c) Density distribution of fluid inclusions in olivine phenocrysts and equivalent pressures in MPa.

systems and extensively debated, neither open- nor closed-system conditions can explain melt inclusion volatile data (e.g. Blundy & Cashman, 2008; Métrich & Wallace, 2008). Several processes have been invoked including the following: (1) secondary post-entrapment evolution of melt inclusions, re-equilibration with their surroundings and H₂O loss induced by proton diffusion (Chen *et al.*, 2011; Gaetani *et al.*, 2012), as a function of the cooling rate (Lloyd *et al.*, 2012); (2) mixing between magma batches with variable extents of degassing (Witham, 2011); (3) magma dehydration by a CO₂-rich gas phase of deep derivation (Spilliart *et al.*, 2006; Métrich *et al.*, 2011). Because of the lower diffusivity of CO₂ with respect to H₂O in basaltic melts at identical temperature (Zhang & Ni, 2010), H₂O is depleted in the melt with respect to CO₂ by kinetic processes.

Percolation of CO₂-rich gas through the volcanic system is evidenced in our samples by the presence of CO₂-rich fluid entrapped in crystals, either as very rare isolated inclusions or more commonly along healed fractures. A process of CO₂-fluxing will enhance both magma dehydration and late-stage re-equilibration of olivine-hosted melt inclusions. Three main points emerge from Fig. 9, in which only melt inclusions hosted in olivine Fo_{≥80} have been plotted. First, the apparent positive correlation between CO₂ and H₂O, which could indicate mixing between magma batches with distinct volatile contents, is an artefact of representation. To avoid such a problem we have recalculated, on the basis of the average value (259) of the H₂O/Ce ratio, the dissolved amount of H₂O in those melt inclusions that were inferred to have lost H₂O (Fig. 7). As a result most inclusions plot on the closed-system degassing curve (CSD¹). Second, two end-members can be identified in the Sc11C sample. They are characterized by distinct H₂O concentrations (1.0 and 1.8 wt %), but exhibit comparable H₂O/Ce ratios. The H₂O-poor melt inclusions have relatively low La, Ce and other incompatible element contents and the lowest La/Sm, La/Yb and K₂O/Na₂O ratios (Table 2). They record total fluid pressures (\leq 160 MPa) that are significantly lower than those deduced from the fluid inclusions (439–526 MPa), and contain a relatively large bubble (25–40 µm in diameter). These observations lead us to conclude that these H₂O-poor inclusions were dominantly affected by diffusive CO₂ loss within the ‘shrinkage’ bubble upon magma ascent, instead of a massive H₂O depletion. Hence, the influence of the internal pressure drop, induced by CO₂ exsolution in the bubble, on the dissolved amount of H₂O would be minimal at low H₂O concentrations, in agreement with Bucholz *et al.* (2013). The variation of CO₂ and H₂O concentrations at nearly constant H₂O/Ce ratio in the Sc11C inclusions would imply distinct C/H ratios in the gas phases. Finally, the highest melt saturation pressure of 470 MPa, although underestimated, is consistent with

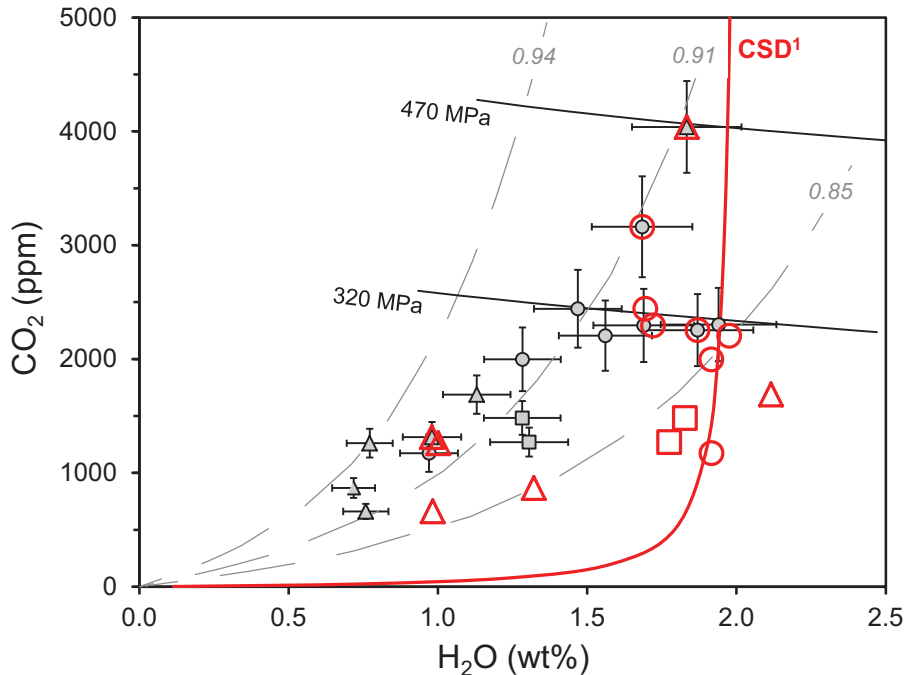


Fig. 9. Variation of H_2O and CO_2 in melt inclusions hosted in olivine Fo_{80-83} . Data uncorrected (grey, filled symbols) and corrected for H_2O depletion (open symbols) rule out mixing between magma batches differing in their volatile contents as the dominant process controlling the CO_2 - H_2O behavior (see text for discussion). Isobars (thick black lines), isopleths (grey dashed lines) and the CO_2 - H_2O degassing curve under closed-system conditions with 1 wt % of free gas phase (CSD^1) are calculated using Papale *et al.* (2006) for QFM redox conditions, a temperature of 1155°C and the composition of Sc1IC-32 a (Electronic Appendix 3). Starting at 550 MPa, the melt dissolves 2 wt % H_2O and 0.51 wt % CO_2 , and more than 95% of the CO_2 is present in the gas phase ($X_{(\text{mol})\text{CO}_2}=0.90$). During decompression under closed-system degassing, the gas phase becomes significantly depleted in H_2O at pressure <100 MPa, when the melt water solubility decreases substantially. The isopleths represent the H_2O - CO_2 evolution in the melt in equilibrium with a gas phase of constant composition. They are calculated for 0.94, 0.91 and 0.85 mole fraction of CO_2 .

the P_{CO_2} values (475–526 MPa) deduced from fluid inclusions and the P_{CO_2} range previously reported for basalts (465–508 MPa) and ultramafic xenoliths (570–586 MPa) from Pico and Faial islands (Zanon & Frezzotti, 2013). We derive the magma ponding depths from our P_{CO_2} determinations (Electronic Appendix 4b), using a density of 2800 kg m^{-3} for the crust and 3210 kg m^{-3} for the underlying mantle, and a possible crustal thickness beneath the Pico–Faial area of about 14 km as estimated from seismic tomography data (Dias *et al.*, 2007). The uncertainty on the depth calculations is difficult to assess because of the uncertainty on the location of mantle–crust transition, which could possibly be as deep as 20 km (Davaille *et al.*, 2005; Zanon & Frezzotti, 2013). Our data indicate a ponding horizon at 15–19 km depth, at which magma is crystallizing; this may represent the mantle–crust interface. Magma batches are subsequently transferred almost directly to the surface with no evidence for long periods of stagnation at shallow crustal levels, as illustrated by the CO_2 density distribution in sample Sc1ID (Fig. 8c), and with no significant degassing of S and Cl before eruption at the surface. High-pressure crystallization and crystal accumulation efficiently contribute to crustal thickening under the Azores, a feature well known in oceanic islands as described, for example, in

the Canary Islands (e.g. Hansteen & Klügel, 2008) and Iceland (e.g. Neave *et al.*, 2013).

Conditions of melting—**inference on mantle source**

Tracking back the composition of the primary magmas in equilibrium with the mantle is critical to estimate the temperature and pressure of melt segregation. Because of magma ponding at the crust–mantle interface, the probability for primary magmas to be erupted is low. Both melt inclusions and lavas testify to high-pressure crystallization involving clinopyroxene. Software allowing the calculations of primary melt composition through the reverse crystallization process usually works well for basalts evolving along the olivine–liquid line of descent, but any removal of clinopyroxene will bias the results. Using PRIMELT2.XLS software (Herzberg & Asimow, 2008) we found that all melt inclusions and most Pico lava samples, including those reported by Beier *et al.* (2012), are compromised by clinopyroxene fractionation. Olivine–clinopyroxene removal is consistent with the positive correlation between Ni and Sc, until ~ 30 ppm Sc and ~ 200 ppm Ni (Fig. 10), whereas higher Ni and Sc concentrations testify to olivine and clinopyroxene accumulation,

respectively. Similarly, K_2O and MgO correlate negatively up to $\sim 10\text{--}11$ wt % MgO , whereas K_2O remains nearly constant at higher MgO values. We thus restricted our selection to lava samples with MgO content of between 10 and 11 wt % and nearly 200 ppm Ni to track back the primary melt composition. PRIMELT2 warns that these samples were affected by clinopyroxene fractionation, except one (Pic24). This latter basalt provided successful solutions, even though most of the selected basalts, with nearly 200 ppm of Ni, were almost suitable candidates within the error limits for major element concentrations.

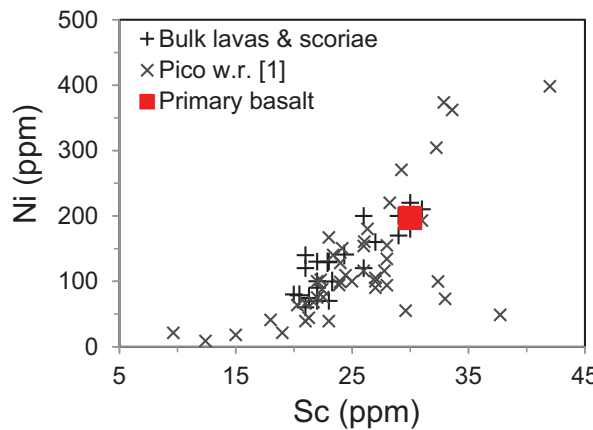


Fig. 10. Variation of Ni vs Sc showing a positive correlation in Pico scoria and lava samples up to ~ 200 ppm Ni. Basalts with ~ 200 ppm Ni and ~ 30 ppm Sc were selected as starting samples for assessing the Pico primary basalt composition using PRIMELT2.XLS software (Herzberg & Asimow, 2008). [I], lava samples from the Pico fissure zone (Beier *et al.*, 2012).

The initial H_2O content (1.27 wt %) was derived from its bulk Ce content and the Ce/ H_2O ratio of 259.

Computations carried out with an Fe^{3+}/Fe_{total} molar ratio of 0.117 ($FeO_{Total} = 10.04$ wt %), for batch primary melts and accumulated fractional primary melts provide closely similar solutions. The resulting primary magma is in equilibrium with olivine $Fo_{91.2}$ at 1362 or 1353°C and contains 15.7 or 15.3 wt % MgO , respectively, before 13–14% olivine fractionation. The inferred potential mantle temperatures (T_p) are 1477 and 1466°C (Electronic Appendix 5) and are consistent with the published data for this island (Beier *et al.*, 2012). More oxidizing conditions cause a significant decrease in both the MgO concentrations and mantle temperatures. We tested the internal consistency of the PRIMELT2 solutions following Herzberg & Asimow (2008). We verified that the initial (P_i) and final (P_f) pressures of melting ($P_i \sim 3$ GPa; $P_f = 3\text{--}2$ GPa), and the melting fraction are comparable in $FeO\text{-MgO}$, $SiO_2\text{-MgO}$ and $CaO\text{-MgO}$ space. Moreover, the estimated pressure of melting of ~ 3 GPa is consistent with the presence of residual garnet in the source (Asimow *et al.*, 2004; Bourdon *et al.*, 2005; Prytulak & Elliott, 2009) as also deduced for Pico basalts (Fig. 11). We also applied the thermo-barometer of Lee *et al.* (2009) for mafic magmas. Calculations using the Pic24 composition ($H_2O = 13$ wt %) indicate primary magmas slightly richer in MgO (~ 17 wt %), but the calculated melting pressure (2.9 GPa) and mantle temperature (1488°C) are comparable with the PRIMELT2 results. The starting magma composition and the redox conditions are critical parameters for these calculations. However, we stress that

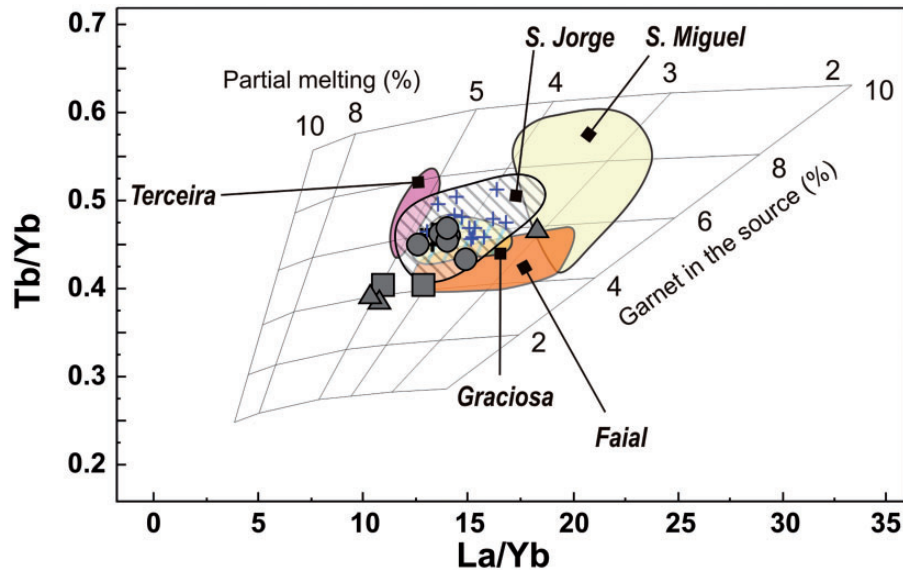


Fig. 11. Tb/Yb vs La/Yb plot with contours redrawn from Bourdon *et al.* (2005) for assessing the degree of partial melting and the amount of residual garnet, assuming fractional melting of a mantle source composed of olivine (55%) orthopyroxene (25%) and variable relative proportions of clinopyroxene and garnet. Melt inclusions representative of the Pico basalts plot in the field of the bulk-rocks indicating 4–5% mantle partial melting. Symbols as in Fig. 3.

the PRIMELT2 solutions indicate a primary melt with an H_2O concentration of $\sim 1.1 \text{ wt } \%$.

Herzberg & Asimow (2008) considered that the driest and hottest Azores magmas represent a melt fraction of ~ 0.07 (7%). Based on a plot of Tb/Yb vs La/Yb , the Pico data (both melt inclusions and lava samples) indicate between 4 and 5% melting of a garnet-bearing mantle source (Fig. 11). Sample Pic24 ($\text{Tb}/\text{Yb} = 0.46$; $\text{La}/\text{Tb} = 14.3$) corresponds to a melt fraction of ~ 0.04 – 0.045 . These values fall in the 0.01 – 0.05 melt fraction range estimated for Pico (Prytulak & Elliott, 2009) and that (0.03–0.05) reported for both the eastern (Beier *et al.*, 2012; Zanon *et al.*, 2013) and western (Genske *et al.*, 2012) Azores islands. For a bulk partition coefficient of 0.01, the mantle source of the Pico magmas ($\text{La}/\text{Sm} = 4$ on average) would contain from 570 to 680 ppm H_2O . These values approach the upper limits for Azores magmas (700 ppm; Asimow *et al.*, 2004).

Geochemical modeling of melt inclusion and bulk lava data provides further evidence for a water-rich mantle source beneath Pico as previously observed for the Azores platform (Schilling *et al.*, 1980). It supports the idea of hydrous decompression melting. Estimation of the thermal anomaly amplitude associated with mantle water enrichment is a critical point, and the assessment of the mantle potential temperature has been highly debated (e.g. Herzberg & Asimow, 2008; White, 2010; Anderson, 2011). Our T_p estimates (1466–1477°C) are consistent with the value of $1443 \pm 24^\circ\text{C}$ reported for the Azores (Courtier *et al.*, 2007). Referring to a MORB T_p of 1350°C (Herzberg & Asimow, 2008), the inferred ΔT for the Azores mantle would be of the order of 120°C or much less ($<50^\circ\text{C}$), whereas mantle plumes are considered to be 100–300°C hotter than normal upper mantle (White, 2010). Melt parcels would segregate from ~ 3 GPa (~ 90 –100 km); this is much shallower than the seismic velocity anomaly depths (200–250 km; Silveira *et al.*, 2006, 2010; Yang *et al.*, 2006).

Mantle water anomaly in the context of the Azores geodynamic setting

The average $\text{H}_2\text{O}/\text{Ce}$ ratio (259 ± 21) determined for Pico basalts is comparable with the average values for submarine non-degassed basalts from the Azores platform (253 ± 33 ; Dixon *et al.*, 2002) and MAR basalts dredged between 35 and 45°N (272 ± 48 ; Michael, 1995), but significantly higher than that reported for southern Atlantic MORB ($\text{H}_2\text{O}/\text{Ce} = 150$; Michael, 1995; Dixon *et al.*, 2002). Variation in the conditions of melting at nearly constant $\text{H}_2\text{O}/\text{Ce}$ ratio does not support the hypothesis of a late stage of water homogenization in magmas at the crust–mantle interface. Consequently, our results reinforce the hypothesis of a mantle H_2O anomaly beneath the Azores region. It is likely that this mantle anomaly has survived for over 10 Myr, as it is recognized in Azores platform

submarine basalts and in the youngest Pico magmas (i.e. olivine-hosted melt inclusions).

The Pico magmas are generated by degrees of melting (4–5%) comparable with all the other Azores islands with the exception of São Miguel (<4%). These estimates must be considered with some caution owing to the possible effects of high-pressure crystal fractionation and the fact that only a few basalts survived clinopyroxene fractionation. However, we stress that the Pico and São Jorge data indicate similar degrees of melting (Fig. 11). They also plot in the same Nd–Sr–Pb isotopic domain of mixing between HIMU and depleted mantle MORB (DMM) mantle sources (Costa *et al.*, 2012). At a larger scale, limited geochemical variability of the mantle source and extents of melting have previously been inferred for the central islands of the Azores archipelago, in contrast to São Miguel (Beier *et al.*, 2010, 2012). Pico basalts have ${}^3\text{He}/{}^4\text{He}$ of 10.5 – $11.2 R_a$, which falls within the range previously published for Azores magmas (Fig. 12) and more specifically for Pico–Terceira–São Jorge basalts (10.5 – $14.5 R_a$; Moreira *et al.*, 1999). These values are higher than those reported for MAR basalts (8.1 – $9.7 R_a$) between 37.26 and 39.57°N (FAZAR expedition), where the most primitive ratio testifies to Azores plume influence (Moreira & Allègre, 2002). FAZAR submarine basalts have variable $\text{H}_2\text{O}/\text{Ce}$ ratios from 177 to 315, with the highest values at 38.5 – 39.9°N (Dixon *et al.*, 2002). Hence helium isotopes and water show a same tendency, even though no proper correlation has yet been established.

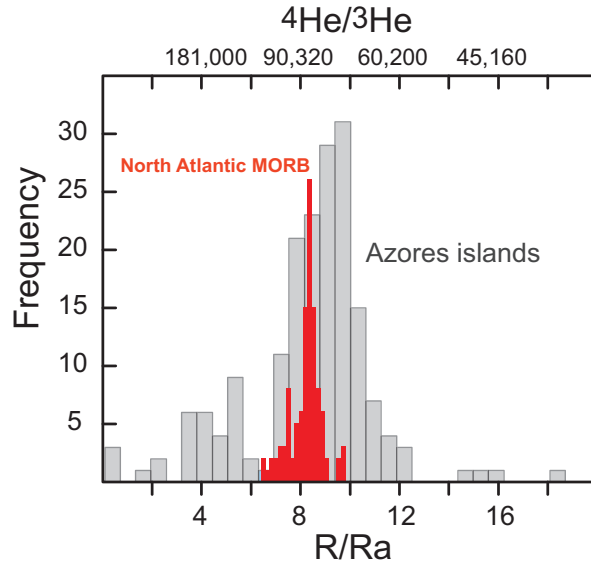


Fig. 12. Histogram of the helium isotopic ratios in lava samples from the Azores archipelago and MORB from the northern Mid-Atlantic ridge. Data from Moreira *et al.* (1999, 2012), Moreira & Allègre (2002), Madureira *et al.* (2005), and Moreira (2013) and references therein.

The important point is that Pico basalts do not record the high R/R_a ratios typical of mantle plumes (up to $39 R_a$ in Loihi pre-shield lavas), but values that are higher than those measured in Hawaii post-shield volcanoes (6·2–9·8 R_a) that in turn are indistinguishable from MORB (Hofmann *et al.*, 2011). Whether the high $^3\text{He}/^4\text{He}$ ratios of ocean island basalts require a low U/Th component or a primitive non-degassed mantle reservoir (rich in ^3He) still gives rise to intense debates (e.g. Anderson, 2011; Hofmann *et al.*, 2011). From new experimental determinations of He bulk partition coefficients ($D_{\text{mineral/melt}}$) for olivine (0·00017) and clinopyroxene (0·0002), Heber *et al.* (2007) have proposed that helium could be less incompatible than its radioactive parents U and Th during mantle melting, resulting in a weak integrated ingrowth of ^4He in the depleted mantle. Lowering of the $^4\text{He}/^3\text{He}$ ratio, which depends on the $^3\text{He}/\text{U}$ ratio, has also been proposed to be linked with the long-term survival of cold, low U/Th, refractory components in the shallow mantle (e.g. Anderson, 2011). We simply point to the fact, here, that trace element data for Pico melt inclusions and bulk rocks do not support the presence of a refractory depleted mantle source component. Old oceanic crust recycling and the presence of dispersed eclogitic material (Hofmann & White, 1982) are consistent with the U–Th isotope data for Pico (Prytulak & Elliott, 2009) and more broadly with He–Pb isotope compositions of Azores basalts (Moreira *et al.*, 1999, 2009).

We propose that the $\text{H}_2\text{O}/\text{Ce}$ ratio of the Azores mantle domain is nearly constant, and that the idea of deepening of the melting source as a result of crustal thickening should be revisited. This latter process would result in deepening of the region of magma ponding and crystallization, but not of the depth of melting. Our data support the idea of a regional mantle enrichment in H_2O , leaving apart São Miguel. Following this line of reasoning, comparable H_2O enrichment could be expected in the mantle source beneath Corvo and Flores on the western side of the MAR. This observation is consistent with the H_2O content ($\sim 0\cdot5\text{--}1\text{ wt } \%$) of the Corvo–Flores primary magmas as indirectly derived from the P – T conditions of basalt evolution (Genske *et al.*, 2012).

These considerations strongly support the hypothesis of decompression melting of a water-rich mantle source as the cause of Azores magmatism, with a relatively low thermal anomaly ($\leq 120^\circ\text{C}$) with respect to the Mid-Atlantic Ridge and compared with mantle plume values ($100\text{--}300^\circ\text{C}$) as reviewed by White (2010). Negative seismic velocity anomalies have been reported beneath the Azores within the upper 200–250 km of the mantle (Silveira *et al.*, 2006, 2010; Yang *et al.*, 2006), but are also present at depths as great as 450 km, and have been related to the presence of a large, deep-seated mantle plume (e.g. Silveira *et al.*, 2010). On a larger scale, thermal and chemically

heterogeneous upwelling at the core–mantle boundary has been inferred from fluid dynamic modeling (e.g. Davaille *et al.*, 2005) and buoyant mantle upwelling from seismic tomography modeling (Adam *et al.*, 2013). However, the notion developed by these researchers of associated secondary hotspots is more complex for the Azores domain, which is strictly speaking not a hotspot.

It is now fairly well established that the Eurasian–African plate boundary in the Azores was the East Azores Fracture Zone until some millions of years ago [$c. 8\text{ Ma}$ according to Luis *et al.* (1994)]. However, owing to plate motion reconfigurations, this plate boundary has moved to the north, from the East Azores Fracture Zone to the currently active Terceira Rift. Therefore, the East Azores Fracture Zone seems to be at present inactive. Whether or not the Eurasian–African plate boundary is discrete or diffuse is strongly debated. Based on global positioning system (GPS) data, and tectonic and seismic activity, Marques *et al.* (2013) showed that the boundary is diffuse in the northwestern half of the Terceira Rift (encompassing the rift and the volcanic ridges to the south for at least 150 km), and discrete in its southeastern half (comprising the Terceira Rift). Yang *et al.* (2006) suggested that this plate boundary migration would result from plate motion over a mantle plume. However, a simple calculation using an absolute velocity of 22 mm a^{-1} (Gripp & Gordon, 2002) and a hotspot-track length $>330\text{ km}$ [from S. Jorge to the old Azores Triple Junction (ATJ)] shows that the plume was at the old ATJ more than 15 Myr ago. This is inconsistent with the proposed ages for migration (e.g. Luis *et al.*, 1994), and with the ages available for the volcanic ridges of S. Jorge ($<1\text{ Ma}$), and Pico–Faial ($<1\text{ Ma}$) (e.g. Hildenbrand *et al.*, 2008, 2012b). The other possible explanation, which we propose here, is the control of tectonics on melt production, in the form of decompression melting. This hypothesis is supported by combined bathymetric, tectonic and GPS data. The crust between the East Azores Fracture Zone and the Terceira Rift shows a sequence of parallel grabens (Princess Alice, Pico–Faial and S. Jorge grabens), with which the main volcanic ridges are associated. This means that, during plate boundary migration to the north, the crust has been extended to form the grabens. Current GPS data also show that the crust is at present extending up to at least 140 km south of the Terceira Rift (Fernandes *et al.*, 2006; Marques *et al.*, 2013). Therefore, lithospheric extension could trigger decompression melting of water-rich mantle.

CONCLUSIONS

Geochemical data for olivine-hosted melt inclusions, their host scoriae and basaltic lavas emplaced along the Pico fissure zone lead us to draw the following conclusions.

- (1) The basalts extruded along the fissure zone experienced high-pressure fractionation and removal of olivine–clinopyroxene (\pm spinel).
- (2) Fluid-saturation pressures recorded by melt inclusions and P_{CO_2} deduced from fluid inclusions indicate an upper limit for magma ponding at *ca.* 18 km depth (~ 500 MPa), (i.e. the mantle–crust) boundary, whereas the parental melt batches segregate from a garnet-bearing mantle source at 90–100 km depth (~ 3 GPa equivalent pressure).
- (3) Melt inclusions that did not experience any secondary H_2O loss and degassing indicate an initial $\text{H}_2\text{O}/\text{Ce}$ ratio of 259 ± 21 at a constant Ce/La ratio (2.18 ± 0.02).
- (4) The primary melt composition and its water content were calculated using PRIMELT2.XLS software (Herzberg & Asimow, 2008).
- (5) In the geodynamic context of extensional tectonics, the Pico magmas can be generated via decompression melting of an H_2O -enriched mantle source, without the need for a significantly elevated mantle potential temperature.

ACKNOWLEDGEMENTS

We are grateful to J. MacLennan, E. Rose-Koga and J. Prytulak for their comments, which significantly improved the paper, and to J.-L. Devidal for his efficient help in LA-ICP-MS analyses of trace elements.

FUNDING

This work was partly funded by MEGAHazards project (PTDC/CTE-GIX/108149/2008, FCT—Portugal, 2010–2012, Principal Investigator F.O.M.), PLUSYS project (PTDC/CTE-GIX/098836/2008, Principal Investigator V.Z.) and the European Science Foundation (ESF), in the framework of the Research Networking Program MeMoVolc (V.Z. exchange grant). V.Z. was further funded by FRCT through grant 03.1.7.2007.1 (FRCT) (PROEMPREGO Operational Program and Regional Government of the Azores).

SUPPLEMENTARY DATA

Supplementary data for this paper are available at *Journal of Petrology* online.

REFERENCES

- Adam, C., Madureira, P., Miranda, J. M., Lourenço, N., Yoshida, N. M. & Fitzenz, D. (2013). Mantle dynamics and characteristics of the Azores plateau. *Earth and Planetary Science Letters* **362**, 258–271.
- Anderson, D. L. (2011). Hawaii, boundary layers and ambient mantle. Geophysical constraints. *Journal of Petrology* **52**, 1547–1577.
- Asimow, P. D., Dixon, J. E. & Langmuir, C. H. (2004). A hydrous melting and fractionation model for mid-ocean ridge basalts: application to the Mid-Atlantic Ridge near the Azores. *Geochemistry, Geophysics, Geosystems* **5**, doi:10.1029/2003GC000568.
- Beier, C., Haase, K. M., Abouchami, W., Krienitz, M.-S. & Hauff, F. (2008). Magma genesis by rifting of oceanic lithosphere above anomalous mantle: Terceira Rift, Azores. *Geochemistry, Geophysics, Geosystems* **9**, Q12013.
- Beier, C., Stracke, A. & Haase, K. M. (2007). The peculiar geochemical signatures of São Miguel (Azores) lavas: Metasomatised or recycled mantle sources? *Earth and Planetary Science Letters* **259**, 186–199.
- Beier, C., Turner, S., Plank, T. & White, W. (2010). A preliminary assessment of the symmetry of source composition and melting dynamics across the Azores plume. *Geochemistry, Geophysics, Geosystems* **11**, Q02004.
- Beier, C., Haase, K. M. & Turner, S. P. (2012). Conditions of melting beneath the Azores. *Lithos* **144–145**, 1–11.
- Blundy, J. D. & Cashman, K. V. (2008). Petrologic reconstruction of magmatic system variables and processes. In: Putirka, K. D. & Tepley, F. J., III (eds) *Minerals, Inclusions and Volcanic Processes. Mineralogical Society of America and Geochemical Society, Reviews in Mineralogy and Geochemistry* **69**, 179–239.
- Bonatti, E. (1990). Not so hot ‘hot spots’ in the oceanic mantle. *Science* **250**, 107–111.
- Bourdon, B., Turner, S. P. & Ribe, N. M. (2005). Partial melting and upwelling rates beneath the Azores from the U-series isotope perspective. *Earth and Planetary Science Letters* **239**, 42–52.
- Buchholz, C. E., Gaetani, G. A., Behn, M. D. & Shimizu, N. (2013). Post-entrapment modification of volatiles and oxygen fugacity in olivine-hosted melt inclusions. *Earth and Planetary Science Letters* **374**, 145–155.
- Cannat, M., Briais, A., Deplus, C., Escartín, J., Georgen, J., Lin, J., Mercouriev, S., Meyzen, C., Muller, M., Pouliquen, G., Rabain, A. & da Silva, P. (1999). Mid-Atlantic Ridge–Azores hotspot interactions: along-axis migration of a hotspot-derived event of enhanced magmatism 10 to 4 Ma ago. *Earth and Planetary Science Letters* **173**, 257–269.
- Carignan, J., Hild, P., Mevelle, G., Morel, J. & Yeghicheyan, D. (2001). Routine analyses of trace elements in geological samples using flow injection and low pressure on-line liquid chromatography coupled to ICP-MS: A study of geochemical reference materials BR, DR-N, UB-N, AN-G and GH. *Geostandards Newsletter* **25**, 187–198.
- Chen, Y., Provost, A., Schiano, P. & Cluzel, N. (2011). The rate of water loss from olivine-hosted melt inclusions. *Contributions to Mineralogy and Petrology* **162**, 625–636.
- Costa, K. M., Parman, S. W., Saal, A. E., Kelley, K. A., Shimizu, N., Nunes, J. C. & Rose-Koga, E. (2012). Volatile content and distribution in the Azorean mantle plume. San Francisco: AGU Fall Meeting, CA, 3–7 December 2012, Abstract V31D-2812 (2012).
- Courtier, A. M., Jackson, M. G., Lawrence, J. F., Wang, Z., Lee, C. T. A., Halama, R., Warren, J. M., Workman, R., Xu, W., Hirschmann, M. M., Larson, A. M., Hart, S. R., Lithgow-Bertelloni, C., Stixrude, L. & Chen, W. P. (2007). Correlation of seismic and petrologic thermometers suggests deep thermal anomalies beneath hotspots. *Earth and Planetary Science Letters* **264**(1), 308–316.
- Davaille, A., Stutzmann, E., Silveira, G., Besse, J. & Courtillot, V. (2005). Convective patterns under the Indo-Atlantic T box. *Earth and Planetary Science Letters* **239**, 233–252.

- Dias, N. A., Matias, L., Lourenço, N., Madeira, J., Carrilho, F. & Gaspar, J. L. (2007). Crustal seismic velocity structure near Faial and Pico Islands (AZORES), from local earthquake tomography. *Tectonophysics* **445**, 301–317.
- Dixon, J. E. & Pan, V. (1995). Determination of the molar absorptivity of dissolved carbonate in basaltic glass. *American Mineralogist* **80**, 1339–1342.
- Dixon, J. E., Leist, L., Langmuir, C. & Schilling, J. G. (2002). Recycled dehydrated lithosphere observed in plumes influence mid-ocean ridge basalt. *Nature* **420**(28), 385–389.
- Elliott, T., Blichert-Toft, J., Heumann, A., Koetsier, G. & Forjaz, V. H. (2007). The origin of enriched mantle beneath São Miguel, Azores. *Geochimica et Cosmochimica Acta* **71**, 219–240.
- Escartín, J., Cannat, M., Pouliquen, G., Rabain, A. & Lin, J. (2001). Crustal thickness of V-shaped ridges south of the Azores: Interaction of the Mid-Atlantic Ridge (36° – 39° N) and the Azores hot spot. *Journal of Geophysical Research* **106**, 21719–21735.
- Fernandes, R. M. S., Bastos, L., Miranda, J. M., Lourenço, N., Ambrosius, B. A. C., Noomen, R. & Simons, W. (2006). Defining plate boundaries in the Azores region. *Journal of Volcanology and Geothermal Research* **156**, 1–9.
- França, Z. T. M., Tassinari, C. C. G., Cruz, J. V., Aparicio, A. Y., Araña, V. & Rodrigues, B. N. (2006). Petrology, geochemistry and Sr–Nd–Pb isotopes of the volcanic rocks from Pico Island, Azores (Portugal). *Journal of Volcanology and Geothermal Research* **156**, 71–89.
- Gaetani, G. A., O’Leary, J. A., Shimizu, N., Bulcholz, C. E. & Newville, M. (2012). Rapid re-equilibration of H_2O and oxygen fugacity in olivine hosted melt inclusions. *Geology* **40**, 915–918, doi:10.1130/G32992.1.
- Gagnon, J., Fryer, B. J., Samson, I. M. & Williams-Jones, A. E. (2008). Quantitative analysis of certified reference materials by LA-ICP-MS and without an internal standard. *Journal of Analytical Atomic Spectrometry* **23**, 1529–1537.
- Gale, A., Escrig, S., Gier, E. J., Langmuir, C. H. & Goldstein, S. L. (2011). Enriched basalts at segment centers: the Lucky Strike ($37^{\circ}17'N$) and Menez Gwen ($37^{\circ}50'N$) segments of the Mid-Atlantic Ridge. *Geochemistry, Geophysics, Geosystems* **12**(6), Q06016.
- Gale, A., Dalton, C. A., Langmuir, C. H., Su, Y. & Schilling, J. G. (2013). The mean composition of ocean ridge basalts. *Geochemistry, Geophysics, Geosystems*, doi.org/10.1002/ggge.20038.
- Genske, F. S., Turner, S. P., Beier, C. & Schaeffer, B. F. (2012). The petrology and geochemistry of lavas from the western Azores islands of Flores and Corvo. *Journal of Petrology* **53**(8), 1673–1708, doi:10.1093/petrology/egs029.
- Gente, P., Dyment, J., Maia, M. & Goslin, J. (2003). Interaction between the Mid-Atlantic Ridge and the Azores hot spot during the last 85 Myr: Emplacement and rifting of the hot spot-derived plateau. *Geochemistry, Geophysics, Geosystems* **4**, 8514–8537.
- Georgen, J. E. & Sankar, R. D. (2010). Effects of ridge geometry on mantle dynamics in an oceanic triple junction region: Implications for the Azores Plateau. *Earth and Planetary Science Letters* **298**, 23–34.
- Ghiorso, M. S. & Sack, R. O. (1995). Chemical transfer in magmatic processes IV. A revised and internally consistent thermodynamic model for the interpolation and extrapolation of liquid–solid equilibria in magmatic system at elevated temperatures and pressures. *Contributions to Mineralogy and Petrology* **119**, 197–212.
- Gripp, A. E. & Gordon, R. G. (2002). Young tracks of hotspots and current plate velocities. *Geophysical Journal International* **150**, 321–361.
- Hansteen, T. H. & Klügel, A. (2008). Fluid inclusion thermobarometry as a tracer of magmatic processes. In: Putirka, K. D. & Tepley, F. J., III (eds) *Minerals, Inclusions and Volcanic Processes*. Mineralogical Society of America and Geochemical Society, *Reviews in Mineralogy and Geochemistry* **69**, 143–177.
- Heber, V. S., Brooker, R. A., Kelley, S. P. & Wood, B. J. (2007). Crystal–melt partitioning of noble gases (helium, neon, argon, krypton, and xenon) for olivine and clinopyroxene. *Geochimica et Cosmochimica Acta* **71**, 1041–1061.
- Herzberg, C. & Asimow, P. D. (2008). Petrology of some oceanic island basalts: PRIMELT2.XLS software for primary magma calculation. *Geochemistry, Geophysics, Geosystems* **9**, doi:10.1029/2008GC002057.
- Hildenbrand, A., Madureira, P., Marques, F. O., Cruz, I., Henry, B. & Silva, P. (2008). Multi-stage evolution of a sub-aerial volcanic ridge over the last 1.3 Myr: S. Jorge Island, Azores Triple Junction. *Earth and Planetary Science Letters* **273**, 289–298.
- Hildenbrand, A., Marques, F. O., Catalão, J., Catita, C. M. S. & Costa, A. C. G. (2012a). Large-scale active slump of the southeastern flank of Pico Island, Azores. *Geology* **40**, 939–942.
- Hildenbrand, A., Marques, F. O., Costa, A. C. G., Sibrant, A. L. R., Silva, P. M. F., Henry, B., Miranda, J. M. & Madureira, P. (2012b). Reconstructing the architectural evolution of volcanic islands from combined K/Ar, morphologic, tectonic, and magnetic data: the Faial Island example (Azores). *Journal of Volcanology and Geothermal Research* **241**–**242**, 39–48.
- Hofmann, A. W. & White, W. M. (1982). Mantle plumes from ancient oceanic crust. *Earth and Planetary Science Letters* **57**, 421–436.
- Hofmann, A. W., Farnetani, C. G., Spiegelman, M. & Class, C. (2011). Displaced helium and carbon in the Hawaiian plume. *Earth and Planetary Science Letters* **312**, 226–236.
- Jean-Baptiste, P., Allard, P., Coutinho, R., Ferreira, T., Fourré, E., Queiroz, G. & Gaspar, J. L. (2009). Helium isotopes in hydrothermal volcanic fluids of the Azores archipelago. *Earth and Planetary Science Letters* **281**, 70–80.
- Lange, R. & Carmichael, I. S. E. (1990). Thermodynamics properties of silicate liquids with emphasis on density, thermal expansion and compressibility. In: Nicholls, J. & Russell, J. K. (eds) *Modern Methods of Igneous Petrology: Understanding Magmatic Processes*. Mineralogical Society of America, *Reviews in Mineralogy* **24**, 25–64.
- Lee, C.-T. A., Luffi, P., Plank, T., Dalton, H. A. & Leeman, W. P. (2009). Constraints on the depths and temperatures of basaltic magma generation on Earth and other terrestrial planets using new thermobarometers for mafic magmas. *Earth and Planetary Science Letters* **279**, 20–33.
- Lloyd, A., Plank, T., Ruprecht, P., Hauri, E. & Rose, W. (2012). Volatile loss from melt inclusions in pyroclast of different sizes. *Contributions to Mineralogy and Petrology*, doi:10.1007/s00410-012-0800-2.
- Luis, J. F., Miranda, J. M., Galdeano, A., Patriat, P., Rossignol, J. C. & Victor, L. A. M. (1994). The Azores triple junction evolution since 10 Ma from an aeromagnetic survey of the Mid-Atlantic Ridge. *Earth and Planetary Science Letters* **125**, 439–459.
- Luis, J. F., Miranda, J. M., Galdeano, A. & Patriat, P. (1998). Constraints on the structure of the Azores spreading center from gravity data. *Marine Geophysical Researches* **20**, 157–170.
- Madeira, J. & Brum da Silveira, A. (2003). Active tectonics and first paleoseismological results in Faial, Pico and S. Jorge Islands (Azores, Portugal). *Annals of Geophysics* **46**, 733–761.
- Madureira, P., Moreira, M., Mata, J. & Allègre, C. J. (2005). Primitive helium and neon isotopes in Terceira Island (Azores archipelago). *Earth and Planetary Science Letters* **233**, 429–440.
- Marques, F. O., Catalão, J. C., DeMets, C., Costa, A. C. G. & Hildenbrand, A. (2013). GPS and tectonic evidence for a diffuse plate boundary at the Azores Triple Junction. *Earth and Planetary Science Letters* **381**, 177–187.

- McDonough, W. F. & Sun, S. S. (1995). The composition of the Earth. *Chemical Geology* **120**, 223–253.
- Mercier, M., Di Muro, A., Métrich, N., Giordano, D., Belhadj, O. & Mandeville, C. W. (2010). Spectroscopic analysis (FTIR, RAMAN) of water in mafic and intermediate glasses and glass inclusions. *Geochimica et Cosmochimica Acta* **74**, 5641–5656, doi:10.1016/j.gca.2010.06.020.
- Métrich, N. & Wallace, P. (2008). Volatile abundances in basaltic magmas and their degassing paths tracked by melt inclusions. In: Putirka, K. D. & Tepley, F. J., III (eds) *Minerals, Inclusions and Volcanic Processes. Mineralogical Society of America and Geochemical Society, Reviews in Mineralogy and Geochemistry* **69**, 363–402.
- Métrich, N., Allard, P., Bertagnini, A. & Di Muro, A. (2011). Comment on ‘Conduit convection, magma mixing, and melt inclusion trends at persistently degassing volcanoes’ by F. Witham *EPSL* (2011) **301**, 345–352. *Earth and Planetary Science Letters* **306**, 306–308, doi:10.1016/j.epsl.2010.11.017.
- Michael, P. J. (1995). Regionally distinctive sources of depleted MORB: Evidence from trace elements and H₂O. *Earth and Planetary Science Letters* **131(3–4)**, 301–320.
- Moreira, M. (2013). Noble gas constraints on the origin and evolution of Earth’s volatiles. *Geochemical Perspectives* **2(2)**, 1–399.
- Moreira, M. & Allègre, C.-J. (2002). Rare gas systematics on Mid Atlantic Ridge (37°40'N). *Earth and Planetary Science Letters* **198**, 401–416.
- Moreira, M., Doucelance, R., Dupré, B. & Allègre, C. J. (1999). Helium and lead isotope geochemistry in the Azores. *Earth and Planetary Science Letters* **169**, 189–205.
- Moreira, M., Rose-Koga, E. F., Koga, K. T., Vlastelic, I., Shimizu, N. & Whitehouse, M. (2009). Correlations between Pb isotopes and volatile elements in melt inclusions from São Miguel, Azores. *EOS Transactions, American Geophysical Union* **90(52)**, Fall Meeting, Abstract V42b-07.
- Moreira, M., Kanzari, A. & Madureira, P. (2012). Helium and neon isotopes in São Miguel island basalts, Azores Archipelago: new constraints on the ‘low ³He’ hotspot origin. *Chemical Geology* **322–323**, 91–98.
- Neave, D. A., Passmore, E., MacLennan, J., Fitton, G. & Thordarson, T. (2013). Crystal–melt relationships and the record of deep mixing and crystallization in the AD 1783 Laki eruption, Iceland. *Journal of Petrology* **54**, 1661–1690.
- Papale, P., Moretti, R. & Barbato, D. (2006). The compositional dependence of the saturation surface of H₂O + CO₂ fluids in silicate melts. *Chemical Geology* **29**, 78–95.
- Parman, S. W. (2007). Helium isotopic evidence for episodic mantle melting and crustal growth. *Nature* **446**, 900–904.
- Prytulak, J. & Elliott, T. (2009). Determining melt productivity of mantle sources from ²³⁸U–²³⁰Th and ²³⁵U–²³¹Pa disequilibrium; an example from Pico Island, Azores. *Geochimica et Cosmochimica Acta* **73**, 2103–2122.
- Richet, P., Whittington, A., Holtz, F., Behrens, H., Ohlhorst, S. & Wilke, M. (2000). Water and the density of silicate glasses. *Contributions to Mineralogy and Petrology* **38**, 337–347.
- Schilling, J. G. (1975). Azores mantle blob: Rare-earth evidence. *Earth and Planetary Science Letters* **25**, 103–115.
- Schilling, J. G., Bergeron, M. B. & Evans, R. (1980). Halogens in the mantle beneath the North Atlantic. *Philosophical Transactions of the Royal Society of London, Series A* **297**, 147–178.
- Shishkina, T. A., Botcharnikov, R. E., Hotz, F., Almeev, R. R. & Portnyagin, M. V. (2010). Solubility of H₂O- and CO₂-bearing fluids in tholeiitic basalts at pressures up to 500 MPa. *Chemical Geology* **77**, 115–125.
- Silveira, G., Stutzmann, E., Davaille, A., Montagner, J. P., Mendes-Victor, L. & Sebai, A. (2006). Azores hotspot signature in the upper mantle. *Journal of Volcanology and Geothermal Research* **156**, 23–34.
- Silveira, G., Vinnik, L., Stutzmann, E., Farra, V., Kiselev, S. & Morais, I. (2010). Stratification of the Earth beneath the Azores from P and S receiver functions. *Earth and Planetary Science Letters* **299**, 91–103.
- Span, R. & Wagner, W. (1996). A new equation of state for carbon dioxide covering the fluid region from the triple point temperature to 1100 K at pressures up to 800 MPa. *Journal of Physical and Chemical Reference Data* **25**, 1509–1596.
- Spillaert, N., Allard, P., Métrich, N. & Sobolev, A. V. (2006). Melt inclusion record of the conditions of ascent, degassing and extrusion of volatile-rich alkali basalt during the powerful 2002 flank eruption of Mount Etna (Italy). *Journal of Geophysical Research* **111**, B04203, doi:10.1029/2005JB003934.
- Stern, S. M. & Pitzer, K. S. (1994). An equation of state for carbon dioxide valid from zero to extreme pressures. *Contributions to Mineralogy and Petrology* **117**, 362–374.
- Stretch, R. C., Mitchell, N. C. & Portaro, R. A. (2006). A morphometric analysis of the submarine volcanic ridge south-east of Pico Island, Azores. *Journal of Volcanology and Geothermal Research* **156**, 35–54.
- Toplis, M. J. (2005). The thermodynamics of iron and magnesium partitioning between olivine and liquid: criteria for assessing and predicting equilibrium in natural and experimental systems. *Contributions to Mineralogy and Petrology* **149**, 22–39.
- Turner, S., Hawkesworth, C., Rogers, N. & King, P. (1997). U–Th isotope disequilibria and ocean island basalt generation in the Azores. *Chemical Geology* **139**, 145–164.
- Van Achterbergh, E., Ryan, C. G., Jackson, S. E. & Griffin, W. (2001). Data reduction software for LA-ICP-MS. In: Sylvester, P. (ed.) *Laser Ablation ICP-MS in Earth Science: Principles and Applications. Mineralogical Association of Canada, Short Course Series* **29**, 239–243.
- Vogt, P. R. (1979). Global magmatic episodes: new evidence and implications for the steady-state mid-oceanic ridge. *Geology* **7**, 93–98.
- White, W. M. (2010). Oceanic island basalts and mantle plumes. The geochemical perspective. *Annual Review of Earth Sciences* **38**, 133–160.
- White, W. M. & Schilling, J. G. (1978). The nature and origin of geochemical variation in Mid-Atlantic Ridge basalts from the Central North Atlantic. *Geochimica et Cosmochimica Acta* **42**, 1501–1516.
- Witham, F. (2011). Conduit convection, magma mixing, and melt inclusion trends at persistent degassing volcanoes. *Earth and Planetary Science Letters* **301**, 345–352, doi:10.1016/j.epsl.2010.11.017.
- Yang, T., Shen, Y., van der Lee, S., Solomon, S. C. & Hung, S.-H. (2006). Upper mantle structure beneath the Azores hotspot from finite-frequency seismic tomography. *Earth and Planetary Science Letters* **250**, 11–26.
- Zanon, V. & Frezzotti, M.-L. (2013). Magma storage and ascent conditions beneath Pico and Faial islands (Azores Islands). A study of fluid inclusions. *Geochemistry, Geophysics, Geosystems*, doi:10.1002/ggge.20221.
- Zanon, V., Kueppers, U., Pacheco, J. M. & Cruz, I. (2013). Volcanism from fissure zones and the Caldeira central volcano of Faial Island, Azores archipelago: geochemical processes in multiple feeding systems. *Geological Magazine* 1–20, doi:10.1017/S0016756812000702.
- Zhang, Y. & Ni, H. (2010). Diffusion of H, C and O components in silicate melts. In: Zhang, Y. & Cherniak, D. J. (eds) *Diffusion in Minerals and Melts. Mineralogical Society of America and Geochemical Society, Reviews in Mineralogy and Geochemistry* **72**, 171–225.